Seryl-butyrate: a prodrug that enhances butyrate's oral bioavailability and suppresses autoimmune arthritis and experimental autoimmune encephalomyelitis

Shijie Cao[1], Erica Budina[1], Michal M. Raczy[1], Ani Solanki[1,2], Mindy Nguyen[1,2], Kevin Hultgren[1], Phillip Ang[1], Joseph W. Reda[1], Lucas S. Shores[1], Ishita Pillai[1], Rachel P. Wallace[1], Arjun Dhar[1], Elyse A. Watkins[1], Jeffrey A. Hubbell[1.3.4]*

[1]Pritzker School of Molecular Engineering, University of Chicago, Chicago, IL 60637, United States

[2]Animal Resource Center, University of Chicago, Chicago, IL 60637, United States

[3]Committee on Immunology, University of Chicago, Chicago, IL 60637, United States

[4]Committee on Cancer Biology, University of Chicago, Chicago, IL 60637, United States

*Corresponding author: Jeffrey A. Hubbell, jhubbell@uchicago.edu

Abstract

Butyrate, a metabolite produced by commensal bacteria, has been intensively studied for its immunomodulatory effects on various immune cells, including T regulatory cells, macrophages, and dendritic cells. Butyrate's development as a drug has been limited by its poor oral bioavailability due to its rapid metabolism in the gut, its low potency and thus high dosing, and its foul smell and taste. By simply esterifying butyrate to serine (SerBut), a design based on the concept of utilizing amino acid transporters to escape the gut and enhance systemic uptake thus increasing bioavailability, we developed an odorless and tasteless compound for oral administration. In the collagen antibody-induced arthritis (CAIA) and experimental autoimmune encephalomyelitis (EAE) murine models of rheumatoid arthritis and multiple sclerosis, we demonstrated that SerBut significantly ameliorated disease severity, modulated key immune cell populations both systemically and in disease-associated tissues, and reduced inflammatory responses without compromising global immune response to vaccination. Our findings highlight SerBut as a promising next-generation therapeutic agent for autoimmune and inflammatory diseases.

Introduction

The gut microbiome has been associated with numerous diseases, with one of the key mechanisms involving immune regulation through the production of microbial metabolites[1–4]. Among these metabolites, short-chain fatty acids (SCFAs), such as butyrate, have gained significant attention due to their anti-inflammatory and immunomodulatory properties[5–7]. Derived from the microbial fermentation of dietary fiber in the colon, butyrate serves as a primary energy source for colonocytes and maintains intestinal homeostasis[5,8]. It is essential for protecting intestinal barrier function by facilitating tight junction assembly[9,10]. As an epigenetic modulator, butyrate is a histone deacetylase (HDAC) inhibitor and can thus alter chromatin structures and regulate gene expression[11–13]. Through HDAC inhibition, butyrate has been shown to upregulate forkhead box P3 (Foxp3) — a transcription factor involved in the development and function of regulatory T cells (Tregs) — as well as suppress nuclear factor κB (NFκB) activation, inhibit the production of interferon γ (IFNγ), and upregulate peroxisome proliferator-activated receptor γ (PPARγ)[14–17]. In addition to its broad anti-inflammatory activity, butyrate affects immune cell migration, adhesion, cytokine expression, proliferation, activation, and apoptosis[18]. Apart from HDAC inhibition, butyrate can also exert anti-inflammatory effects on immune cells, such as dendritic cells and Tregs, via signaling through specific G-protein coupled receptors (GCPRs): GPR41, GPR43, and GPR109A[19–22]. Collectively, these properties of butyrate hold significant potential for the development of therapeutic strategies, particularly in the treatment of immunological disorders, including autoimmune diseases.

Autoimmune diseases, affecting nearly 5% of the global population, have increased in prevalence over the last few decades[23]. These disorders arise when the immune system mistakenly attacks the body's own cells and tissues, resulting in chronic inflammation and tissue damage. The onset of autoimmune diseases may be influenced by a combination of genetic and environmental factors. Recent studies have underscored the pivotal role of the gut microbiome in modulating immune responses and influencing the development and progression of

autoimmune diseases[3]. For instance, dysregulation of the gut microbiome, or dysbiosis, has been implicated in the pathogenesis of rheumatoid arthritis and multiple sclerosis[24–27]. Current therapeutics for autoimmune diseases, such as immunosuppressive agents, can provide symptom relief but often do not address underlying causes of these complex disorders. There is accumulating evidence that microbial metabolites, such as SCFAs, can impact the immune system and contribute to the development or regulation of autoimmune diseases[28]. Consequently, these findings highlight the potential of using microbial metabolites as therapeutic agents to treat autoimmune diseases by targeting the underlying mechanisms and modulating the immune response.

In spite of this promise, oral administration of sodium butyrate has faced challenges due to its foul and persistent odor and taste, even when administered with enteric coatings or encapsulation. Moreover, butyrate is not absorbed in the gut regions where it could exert therapeutic effects and is rapidly metabolized in the gut as an energy source, limiting its pharmacological impact[29]. Alternative routes of butyrate administration, such as intrarectal delivery or continuous intravenous infusion, are often deemed unfeasible for patients with chronic disorders[30–33]. Therefore, there is a need for innovative delivery methods for butyrate, including prodrugs that can enhance its systemic bioavailability.

To overcome these limitations, we sought to develop a prodrug strategy that enables butyrate to bypass metabolism in the gut, enter the bloodstream, and exert its therapeutic effects systemically after liberation. In this study, we designed an L-serine conjugate of butyrate (2-seryl butyrate, or here SerBut) that exploits the gut transport mechanisms of amino acids. Additionally, the conjugation effectively masked the odor and taste of free butyrate, important for facilitating patient compliance for potential clinical applications. We found that SerBut not only enhanced systemic bioavailability, but also facilitated its crossing of the blood-brain barrier (BBB), thereby enabling access to the central nervous system (CNS). In a mouse model of collagen antibody-induced arthritis (CAIA), SerBut treatment showed a significant reduction in

disease progression that was associated with a systemic increase in Tregs and an increase in the ratio of immunoregulatory M2 macrophages to pro-inflammatory M1 macrophages. In an experimental autoimmune encephalomyelitis (EAE) model of multiple sclerosis, SerBut significantly suppressed disease onset and severity, decreased immune cell infiltration in the spinal cord, and upregulated inhibitory markers such as PD-1 and CTLA-4 on $CD4^+$ T cells, increased Tregs, and downregulated activation markers on a variety of myeloid cells in the spinal cord-draining lymph nodes. SerBut treatment did not reduce vaccinal immune responses at either the humoral or cellular levels. Thus, in two disease models, SerBut administration modulated immune responses at both the myeloid and lymphoid levels without unduly blunting protective immune responses.

Results

Conjugation of L-serine to butyrate maintained its biological activity while enhancing oral bioavailability.

We conjugated L-serine to butyryl chloride using trifluoroacetic acid at room temperature, resulting in a 79% yield of the final product, 2-seryl-butyrate (SerBut) (**Fig. 1A, fig. S1**). The conjugation effectively masked the unpleasant odor associated with free sodium butyrate or butyrate acid.

Butyrate is known to regulate myeloid cells, including the inhibition of dendritic cell (DC) maturation in response to pro-inflammatory stimuli[34]. We employed bone marrow-derived dendritic cells (BMDCs) to assess the biological effects of SerBut compared to free sodium butyrate (NaBut) (**Fig. 1B**). BMDCs were first incubated with butyrate formulations for 24 hr, and then stimulated with lipopolysaccharide (LPS) for 18 hr. We found that NaBut exhibited cytotoxicity to BMDCs at butyrate concentrations above 0.5 mM, while SerBut was well tolerated up to 1.8 mM (**Fig. 1C**). Flow cytometry was used to compare the expression of MHC class II, CD80, and CD86 on BMDC surfaces. At the same concentration of 0.2 mM NaBut, SerBut

showed similar suppression levels of MHCII and CD80 (**Fig. 1D, E**). Although SerBut did not suppress CD86 expression as effectively as NaBut at 0.2 mM (**Fig. 1F**), we observed dose-dependent suppression of CD86 with SerBut at higher concentrations (**fig. S2B**). Similarly, SerBut suppressed the secretion of TNFα from BMDCs (**Fig. 1G, fig. S2D**). As demonstrated by suppression of LPS-stimulated BMDC activation, SerBut retains the biological activity of butyrate.

The primary site for amino acid absorption is the small intestine, where amino acid transporters are present in intestinal epithelial cells[35]. We conducted a biodistribution study to determine whether conjugating L-serine to butyrate enhances oral butyrate absorption and bioavailability. We measured free butyrate levels in plasma and several major organs after oral gavage of SerBut and compared them with NaBut (**Fig. 1H**). We found that SerBut significantly increased plasma butyrate levels at 3 hr after oral administration compared to NaBut. In the liver, where orally administered drugs enter directly through the hepatic portal circulation, we observed elevated butyrate levels in mice treated with SerBut but not NaBut. In secondary lymphoid organs, we observed elevated butyrate in the mesenteric lymph nodes (mLNs) and spleen. Butyrate levels were also elevated in lungs at 3 hr post-administration of SerBut.

L-serine is an amino acid known to cross the BBB via the sodium-dependent system A and the sodium-independent alanine, serine, and cysteine transport system[36,37]. Montaser et al. showed that utilizing the L-type amino acid transporter 1 enhances the efficient delivery of small prodrug across the BBB[38]. Therefore, we investigated whether L-serine conjugation could assist butyrate in entering the CNS, including the spinal cord and brain. Our findings revealed that SerBut significantly increased butyrate levels in both the spinal cord (a remarkable level of approximately 43% that in the liver, as compared in micrograms of butyrate per gram of tissue) to even brain (to approximately 6%), whereas no exposure was observed after administration with NaBut (**Fig. 1H**).

SerBut suppresses collagen antibody-induced arthritis (CAIA) in mice.

The composition of gut microbiota have been shown to affect the development of rheumatoid arthritis (RA)[24,25,39]. Previous research has shown that butyrate can improve RA symptoms by targeting key immune cells such as osteoclasts and T cells[40]. Furthermore, studies have demonstrated that butyrate supplementation effectively reduces arthritis severity in animal models by modulation of regulatory B cells[41]. Given SerBut's enhanced accumulation in crucial immune tissues following oral administration, we sought to evaluate its efficacy in the CAIA mouse model (**Fig. 2A**). This model is induced by passive immunization with a cocktail of anti-collagen antibodies followed by LPS, which triggers a cascade of innate immune cell infiltration to the joints leading to inflammation and swelling within one week of immunization.

Mice were pretreated with SerBut or PBS once daily by oral gavage, beginning two weeks before the induction of arthritis. We observed that SerBut treatment significantly suppressed the development of arthritis in treated mice. In contrast, PBS-treated mice exhibited severe inflammation in the fore- and hindpaws, demonstrated by their increasing clinical scores over time and the measurements of paw thickness (**Fig. 2B-E**). Histological analysis revealed that oral administration of SerBut effectively suppressed inflammatory responses in the paws and reduced joint pathology compared to PBS-treated mice (**Fig. 2F, G**). In the CAIA model, anti-collagen antibodies binding to joint cartilage activates complement proteins, leading to the recruitment of immune cells such as macrophages and T cells to the affected joints[42,43]. This immune cell infiltration contributes to joint inflammation, tissue damage, and the clinical manifestations of arthritis. In our study, we observed that SerBut treatment effectively reduced immune cell infiltration into the joints (**Fig. 2F, fig. S4**). Additionally, anti-collagen antibodies specifically target and degrade collagens in the joints, causing cartilage integrity and joint function loss, ultimately leading to arthritis symptoms[44]. We found that SerBut treatment also prevented collagen loss in the joints (**Fig. 2G, fig. S5**), suggesting that SerBut may have

therapeutic potential in mitigating joint damage and preserving collagen content in the autoimmune arthritis.

To better understand the immunomodulatory effects of SerBut in CAIA, we analyzed immune cell populations in the spleen and hock-draining LNs using flow cytometry. Our results showed that SerBut treatment increased Foxp3 expression in both $CD4^+$ and $CD8^+$ T cells in the spleen (**Fig. 2H, I**), indicating that SerBut induced systemic Tregs in the RA disease setting. In the hock-draining LNs (**Fig. 2J**), SerBut significantly reduced the proportion of Th17 cells, as evidenced by the decreased percentage of $ROR\gamma t^+$ $CD4^+$ T cells. Additionally, we observed a significant increase in IL-10-producing B cells within the hock-draining LNs (**Fig. 2K**), which play a vital role in maintaining immune homeostasis[41,45]. Finally, the hock-draining LNs also demonstrated upregulation in Arg-1 expression in macrophages (**Fig. 2L**), leading to an increased M2($Arg1^+$)/M1($iNOS^+$) macrophage ratio in the hock-draining LNs (**Fig. 2M**). The shift towards a higher proportion of immunoregulatory M2 macrophages suggests that SerBut promotes a more balanced immune response, which may be crucial for suppressing inflammation in the paws and reducing joint damage in the context of RA. Overall, these findings highlight the potential therapeutic utility of SerBut in treating RA by modulating the immune system at both the innate and adaptive levels, mitigating disease symptoms.

SerBut suppresses EAE development through modulation of T cells and myeloid cells in the spinal cord-draining LNs.

Multiple sclerosis (MS) is an autoimmune disease in which T cells are reactive to myelin autoantigens, resulting in a chronic demyelinating inflammation in the CNS. Evidence suggests a connection between gut microbiota and MS[26,27,46–50], particularly dysbiosis in the gut microbiota of MS patients, which includes a reduction of SCFA-producing bacteria[51]. Oral administration of SCFAs, such as butyrate, has been shown to alleviate the severity of EAE, a mouse model of MS, by reducing Th1 cells and an increase in Tregs[28,52]. Butyrate has also

been demonstrated to ameliorate demyelination and enhance remyelination in a mouse model of cuprizone-induced demyelination[53]. Our biodistribution study revealed that SerBut significantly increased butyrate levels in the brain and spinal cord, in addition to the lymphatic tissues, suggesting its potential in treating MS.

We assessed the efficacy of SerBut in suppressing EAE development. To minimize physiological stress from daily oral gavage, mice were given drinking water containing 100 mM SerBut for the two weeks preceding disease induction and were subsequently administered 24 mg SerBut via oral gavage once daily (**Fig. 3A**). SerBut treatment significantly reduced the EAE clinical score in treated mice (**Fig. 3B**), indicating disease symptom alleviation. The treatment also delayed EAE onset, as shown by the lower percentage of SerBut-treated mice with a disease score greater than 1 (**Fig. 3C**). Neither NaBut nor L-serine at the same molar doses alleviated disease.

A thorough analysis of immune cell populations in the spinal cord-draining LNs (SC-dLNs) showed that SerBut treatment significantly increased PD-1 and CTLA-4 expression on $CD4^+$ T cells, expanded Tregs, and upregulated CTLA-4 expression on $CD4^+$ Tregs (**Fig. 3D-H**). These results suggest that SerBut may help suppress excessive immune responses during EAE by modulating key immune checkpoints and regulatory T cell populations. Additionally, in the SC-dLNs, SerBut treatment reduced the number of myelin oligodendrocyte glycoprotein (MOG)-specific T cells and MOG^+ $ROR\gamma t^+$ $CD4^+$ T cells (Th17 cells), antigen-specific pathogenic cells that contribute to EAE development (**Fig. 3I, J**). SerBut treatment also increased Foxp3, PD-1, and CTLA-4 expression on these MOG^+ $CD4^+$ T cells (**Fig. 3K-M**), potentially preventing these cells from promoting inflammation and tissue damage in EAE. Consistent with disease readouts, neither NaBut nor L-serine induced any changes to these cellular immune responses.

From the innate immune perspective, SerBut treatment reduced the expression of co-stimulatory markers, including CD40 and CD86, as well as the antigen-presenting molecule MHC class II, on various myeloid cells such as $CD11b^+CD11c^-$ cells, $CD11b^+F4/80^+$

macrophages, $CD11c^+$ dendritic cells, $CD11b^+CD11c^+$ dendritic cells, and $CD11b^+Ly6C^+Ly6G^-$ myeloid-derived suppressor cells (MDSCs) (**Fig. 3N**, **Fig. S9**). As these myeloid cells play a crucial role in initiating and propagating immune responses, the reduction of co-stimulatory molecules and MHC class II expression on these cells suggests that SerBut treatment may inhibit their activation and function. This could lead to a dampening of the inflammatory response and contribute to EAE suppression. MDSCs are reported to have immunosuppressive functions, such as inhibiting T cell proliferation and promoting Treg expansion, in the context of EAE[54,55]. We observed not only a downregulation of activation markers on these cell types but also a significant increase in the percentage of these cells in both SC-dLNs and mesenteric LNs (**Fig. S10**). Overall, our results demonstrate that SerBut has a significant therapeutic impact on EAE by modulating the activity of various immune cell populations and reducing inflammatory responses. All these effects were observed exclusively with SerBut treatment and not with free L-serine nor NaBut, suggesting the importance of conjugation in enhancing butyrate's systemic and possibly CNS bioavailability.

SerBut administered post-EAE induction suppresses disease progression and inhibits immune responses in the spinal cord

We next sought to investigate whether administration of SerBut post-EAE induction could also suppress disease progression and induce immunological changes in the spinal cord. Mice were given twice-daily gavage of SerBut after EAE induction (**Fig. 4A**). We observed that the SerBut-treated mice had significantly lower EAE clinical scores compared to PBS-treated mice (**Fig. 4B**). Only 2 out of 8 mice in the SerBut-treated group developed EAE with scores higher than 1 by the end of the study, and the rest remained healthy throughout the experiment (**Fig. 4C**). Additionally, PBS-treated mice began to experience a significant drop in body weight starting on day 14, whereas the SerBut-treated mice continued to grow over time (**Fig. 4D**).

When PBS-treated mice reached a plateau in disease score, we sacrificed both groups and examined the spinal cords to assess the impact of treatment. From immunofluorescence images with anti-CD45 and anti-myelin basic protein (MBP) staining, we observed substantial immune cell infiltration into the spinal cords of PBS-treated mice, but not in SerBut-treated mice (**Fig. 4E**, **Fig. S12**). The two mice from the SerBut-treated group that did not respond to treatment also showed corresponding immune cell infiltration into their spinal cords (**Fig. S12**). We further homogenized part of the spinal cord and measured IFNγ levels, noticing a decrease in IFNγ in the spinal cords of SerBut-treated mice (**Fig. 4F**).

We also quantified the effect of SerBut treatment on the immune cell compartment in the spinal cord using flow cytometry. We observed a decrease in immune cell populations across most immune cell types in the spinal cord, including $CD45^+$ cells, $CD3^+$ T cells, and pathological Th17 cells ($ROR\gamma t^+$ $CD4^+$ T cells) (**Fig. 4G-I**), as well as macrophage-like $CD11b^+CD11c^-$ and $CD11b^+F4/80^+$ cells (**Fig. 4J-K**). We did not observe a significant reduction in the $CD11c^+$ DC population (**Fig. 4L**); however, there was a decrease in MHC class II on their surface, as well as on $CD11b^+CD11c^-$ cells, indicating diminished activation of these cells in the spinal cords of SerBut-treated mice (**Fig. 4M-O**). The reduced MHC class II on the myeloid cells was observed not only in the spinal cord, but also in the mesenteric LNs (**Fig. S14**). In this experiment, we also noted that SerBut increased the frequency of $Foxp3^+$ Tregs both systemically in the spleen and locally in the SC-dLNs and mesenteric LNs (**Fig. S15**), consistent with our findings in previous RA and EAE experiments. These findings suggested that SerBut exerts its immunomodulatory effects both systemically and in disease-related tissues.

SerBut does not impact global immune responses to vaccination or alter blood chemistry toxicological markers

Several immune modulators employed in autoimmunity blunt systemic immune responses to vaccination or infection. As a benchmark, we employed fingolimod (FTY720) is a

widely used oral compound for treating MS[56]. FTY720 targets the sphingosine-1-phosphate receptor and affects the immune system by sequestering lymphocytes in lymph nodes, reducing their migration to the CNS and ultimately lowering inflammation[57]. Studies have shown that oral prophylactic administration of fingolimod to animals with EAE induction completely prevents the development of EAE, while therapeutic administration reduces the severity of EAE[57]. However, FTY720 can inhibit global immune responses, as demonstrated in our earlier experiment, where FTY720 administration to mice vaccinated with ovalbumin (OVA) and adjuvant prevented the generation of OVA-specific IgG[58].

To gain insight into whether SerBut might impact immune responses to vaccination, we vaccinated mice with OVA, along with the adjuvant alum and monophosphoryl-lipid A (MPLA), which mimics the clinical vaccine adjuvant AS-04, through subcutaneous injections in the hock. Mice were treated with either PBS, SerBut, or FTY720 by oral gavage (**Fig. 5A**). Blood collected on days 9 and 13 revealed OVA-specific IgG antibody generation in both PBS and SerBut-treated mice but much less so in FTY720-treated mice, indicating that FTY720, unlike SerBut, suppressed humoral responses to the OVA vaccination (**Fig. 5B, C**). To evaluate cellular responses, we sacrificed the mice and isolated immune cells from hock-draining LNs. FTY720 reduced B cell ($CD19^+B220^+$), T cell ($CD3^+$), and $CD4^+$ T cell populations in both hock-draining LNs and the spleen (**Fig. 5D-F, fig. S15**). Interestingly, FTY720 substantially increased Foxp3 Tregs in both LNs and the spleen (**Fig. 5G, fig. S17**). When we restimulated splenocytes isolated from mice with OVA *in vitro*, we observed a significant reduction in cytokine production, including TNFα, IFNγ, IL-6, IL-5, IL-13, and IL-10 (**Fig. 5H-M**), indicating that FTY720 suppressed antigen-specific T cell responses to OVA. In contrast, SerBut treatment did not suppress these cellular responses, although interestingly, we did observe some significant increases in IL-6, IL-5, IL-13, and IL-10 production with SerBut treatment.

We also conducted serum biochemistry analysis on the mice to determine if the treatment induced any organ toxicity other than effects on immune responses (**Fig. S18**). In

general, we did not see significant changes for the major readouts from the panel upon SerBut treatment, including markers of liver, pancreas, and kidney toxicity. FTY720 induced a modest reduction in blood urea nitrogen levels but no other changes. Overall, these findings suggest that SerBut does not have a major impact on global immune responses to vaccination and is safe for mice when given via twice-daily oral gavage.

Discussion

In this study, we investigated the therapeutic potential of SerBut in treating RA and MS using CAIA and EAE as murine models. Orally administered free butyrate can be absorbed and quickly metabolized by host tissues and cells via butyryl-CoA/acetate CoA transferase and phosphotransbutyrylase-butyrate kinase pathways[59]. In the colon, butyrate is primarily consumed by the colonocytes as an energy source[29]. By employing a simple chemical strategy to conjugate serine to butyrate, we improved the oral bioavailability of butyrate including into the CNS, creating a prodrug candidate that offers several advantages, including a lack of unpleasant odor and taste, and higher efficacy compared to free butyrate. Our results demonstrated that SerBut significantly ameliorated the severity of both diseases, modulated key immune cell populations, and reduced inflammatory responses, all without compromising global immune responses to vaccination.

Butyrate, a key metabolite from commensal bacteria, has multiple modulating effects across different types of immune cells. It has been shown to facilitate peripheral generation of Tregs through both direct upregulation of Foxp3 by HDAC inhibition[16,17], and indirect effects from the induction of tolerogenic DCs[19,60]. In our study, we demonstrated that SerBut treatment increased peripheral Tregs in both CAIA and EAE settings, as well as in both local LNs and spleen (**Fig. 2H**, **3F, K**, **fig. S8B**, **S15**). Notably, we observed enhanced biodistribution of SerBut in these tissues after oral administration, which is not limited to gut tissues as previously reported[61,62]. Butyrate has also been shown to modulate the differentiation of macrophages and

DCs. Through HDAC inhibition, butyrate downregulates LPS-induced proinflammatory cytokines produced by macrophages[63], and activates macrophage metabolism towards oxidative phosphorylation through upregulation of Arg-1, promoting an anti-inflammatory M2 phenotype[64]. In our CAIA model, enhancing the systemic bioavailability of butyrate through SerBut significantly increased the M2/M1 macrophage ratio in hock-draining LNs, which could exert direct anti-inflammatory effects on paw and joint inflammation. Moreover, butyrate has been shown to suppress DC activation and induce tolerogenic DCs through a combination of signaling via GPR109A and HDAC inhibition[19]. In our study, we observed a similar effect from SerBut compared to free NaBut in suppressing LPS-induced activation, including co-stimulatory markers CD80 and CD86, and MHC class II expression of BMDCs isolated from mice. Consistently, in the EAE model, we observed downregulation of these costimulatory markers and MHC class II on various myeloid cells across different tissues, suggesting the important roles butyrate can play in suppressing disease progression through this pathway while delivered systemically.

Myeloid cells, such as DCs and macrophages, play a crucial role in antigen presentation and T cell activation. For instance, CD86 interacts with CD28 on T cells, promoting their activation and proliferation[65,66]. CTLA-4 is a surface receptor predominantly expressed on T cells, particularly on Tregs, and competes with CD28 for binding to CD86 on myeloid cells, delivering an inhibitory signal to T cells[67]. Intriguingly, in our EAE experiment, we observed that SerBut treatment led to a significant increase in CTLA-4 expression on both total $CD4^+$ T cells, and Tregs in the spinal cord-draining LNs. This concurrent upregulation of CTLA-4 on T cells, and downregulation of CD86 on myeloid cells can synergistically contribute to a more profound suppression of immune activation, ultimately dampening autoimmune responses.

In the EAE experiment, we have shown that twice-daily administration of SerBut significantly reduces immune cell infiltration into the spinal cord. We do not know if this CNS effect is modulated directly as a result of the butyrate that crosses the BBB or whether its effect

on peripheral immune cells indirectly impacts the CNS. Additionally, the effect of butyrate on BBB (or blood-spinal cord barrier) endothelial cell functions and integrity warrants further investigation.

We have shown that SerBut has several potential benefits over free NaBut for clinical translation: serine conjugation to butyrate masks its odor and taste, yields higher bioavailability, and shows greater efficacy in suppressing autoimmune disease models than NaBut. The dose used in these studies can be converted to 6 grams per dose for human clinical trials, which could be formulated as powder in a packet to stir into drinking water for daily consumption. Importantly, SerBut did not negatively impact global immune responses to vaccination, as demonstrated by the generation of equivalent OVA-specific IgG humoral and cellular immune responses in both PBS and SerBut-treated mice. Although we observed effective immune modulation in the context of autoimmune arthritis and EAE, the immune response elicited by a strong, Th1-biasing adjuvant (the TLR4 agonist MPLA in the alum depot) was sufficient to overcome the effects of SerBut[68].

The findings of our study provide evidence for the potential of SerBut as a next-generation therapeutic agent for RA and MS. Further studies, including preclinical and clinical studies, are needed to better understand the long-term safety and efficacy of SerBut in the context of rheumatoid arthritis, multiple sclerosis, and other autoimmune and inflammatory diseases. Given its broad immunomodulatory effects shown in our study, it would be valuable to explore the potential of SerBut in treating a broader range of immune-related conditions.

Materials and Methods

Study design

The objective of this study was to chemically conjugate L-serine to butyrate to improve butyrate's oral bioavailability and investigate the therapeutic potential of the conjugate, SerBut, in the context of RA and MS using CAIA and EAE murine models.

In the biodistribution study, we quantified the butyrate content in various major organs following oral gavage of SerBut. In the RA model, mice were treated daily with either PBS or SerBut via oral gavage. Paw inflammation was assessed over time, and the pathology of inflamed paws and joints was evaluated using histology. Immune cell population responses were analyzed by flow cytometry after sacrificing the mice at the end of the experiment when consistent RA scores were established. In the EAE model, we compared the efficacy of SerBut, PBS, free butyrate, and free L-serine in suppressing disease progression. Immune responses were evaluated after sacrificing the mice when they reached a plateau in disease scores. In the vaccination study, SerBut was compared with FTY720 regarding their global immunosuppressive effects. The study endpoint was determined based on previous reports that day 13 after OVA immunization was sufficient to induce anti-OVA IgG antibodies[58].

Sample size was determined using results obtained from previous and preliminary studies. At least 5, and in most cases 7-9 independent biological replicates were examined for each group analyzed. See figure legends for details on n for each display figure. All experiments were replicated at least twice. Mice were randomly assigned to treatment groups. The person assessing clinical scores for RA and EAE experiments was separate from the person administering treatment and was blinded to the treatment group. The person performing fluorescent imaging and histology analysis was also blinded to treatment groups. Statistical methods are described in the "Statistical analysis" section.

Synthesis of SerBut

L-Serine (20 g, 0.19 mol) was added to trifluoroacetic acid (200 ml) and the suspension was stirred for 30 min until everything dissolved. Butyryl chloride (25.7 ml, 0.23 mol) was then added to the solution and the mixture was stirred for 2 hr at room temperature. The reaction was then transferred to an ice bath and diethyl ether (500 ml) was added, which resulted in a precipitation of a white solid. The resultant fine white precipitate was collected by filtration,

washed with cold diethyl ether, and dried under vacuum to afford 26.3 g of 2-seryl-butyrate (0.15 mol, 79%). The final product was confirmed by 1H NMR (500MHz, DMSO-d6) [ppm]: 0.88 (3H, t), 1.55 (2H, m), 2.32 (2H, t), 4.30 (1H, t), 4.43 (2H, d), 8.66 (2H, s), 14.06 (1H, s).

Mice

C57BL/6 mice, aged 8-12 weeks, were purchased from Charles River (strain code: 027, Charles River). BALB/c mice, aged 6-10 weeks were purchased from the Jackson Laboratory (strain code: 000651, JAX). C57BL/6 and BALB/c mice were maintained in a specific pathogen-free (SPF) facility at the University of Chicago. Mice were maintained on a 12 hr light/dark cycle at a room temperature of 20-24 °C. All protocols used in this study were approved by the Institutional Animal Care and Use Committee of the University of Chicago.

Flow cytometry and antibodies

Flow cytometry was done using BD LSRFortessa™, and data were analyzed using FlowJo 10.8.0. Antibodies against the following markers were used in the RA and EAE mouse model: INOS (BUV737, Cat#367-5920-82, Invitrogen), CD11c (BV421, Cat#562782, BD Biosciences), Ly6C (BV605, Cat#128036, BioLegend), CD11b (BV711, Cat#101242, BioLegend), Ly6G (AF488, Cat#127626, BioLegend), CD40 (PerCP/Cy5.5, Cat#124624, BioLegend), CD206 (PE, Cat#141706, BioLegend), Arginase 1 (PE-Cy7, Cat#25-3697-82, Invitrogen), F4/80 (APC, Cat#123116, BioLegend), CD86 (AF700, Cat#105024, BioLegend), I-A/I-E (APC/Cy7, Cat#107628, BioLegend), CD19 (BUV396, Cat#563557, BD Biosciences), CD3 (BUV737, Cat#741788, BD Biosciences), CD3 (BV605, Cat#100351, BioLegend), CD4 (BV605, Cat#100548, BioLegend), CD4 (BV711, Cat#100550, BioLegend), PD-1 (BV711, Cat#135231, BioLegend), Foxp3 (AF488, Cat#53-5773-82, Invitrogen), RORγt (PerCP/Cy5.5, Cat#562683, BD Biosciences), CD5 (PE, Cat#100607, BioLegend), CTLA-4 (PE-Cy7, Cat#25-1522-80, Invitrogen), CD25 (APC, Cat#162105, BioLegend), CD8 (AF700, Cat#100730, BioLegend), IL-

10 (APC/Cy7, Cat#505036, BioLegend), CD45 (BUV395, Cat#564279, BD Biosciences), CD45 (V450, Cat#560501, BD Biosciences). The I-A(b) mouse MOG 38-49 GWYRSPFSRVVH (MOG tetramer, PE) was obtained from NIH Tetramer Core Facility.

Mouse BMDC isolation and activation study

Murine BMDCs were collected from 6-week-old female C57BL/6 mice as described by Lutz et al[69]. BMDCs were seeded at 3 x 10^6 total cells/plate in petri dishes. Cells were cultured at 37°C and 5% CO_2 in the media: RPMI 1640 (Life Technologies), 10% HIFBS (Gibco), GM-CSF (20 ng/mL; recombinant Mouse GM-CSF (carrier-free) from BioLegend) , 2 mM l-glutamine (Life Technologies), 1% antibiotic- antimycotic (Life Technologies). Media was replenished on day 3 and day 6. Cells were used on day 9. Isolated BMDCs were plated in round-bottom 96 well plates at 100,000 cells per well in RPMI media and co-cultured with different concentrations of either NaBut or SerBut (from 0.02 to 1.8 mM) for 24 hr. Subsequent to that, LPS (1 µg/mL) was added for another 18 hr. The supernatant of cell culture was collected and analyzed by LEGENDPlex™ to analyze the concentrations of cytokines (BioLegend). BMDC were collected and stained with live/dead stain (Cat#L34957, Invitrogen) and fluorescent antibodies against CD11c (PE-Cy7, Cat#558079, BD Biosciences), MHCII (APC-Cy7, Cat#107628, BioLegend), CD80 (PE, Cat#104708, BioLegend), CD86 (FITC, Cat#MA1-10300, Invitrogen), and were analyzed using flow cytometry (BD LSRFortessa).

Biodistribution of SerBut

C57BL/6 mice were orally administered with 50.4 mg NaBut or 80 mg SerBut (both containing equivalent 40 mg butyrate). At 3 hr post-administration, mice were anesthetized under isoflurane and blood was collected via cheek bleeding, and mice were then transcardially perfused with a minimum of 30 mL PBS containing 1 mM EDTA. Organs, including liver,

mesenteric lymph nodes (mLNs), spleen, lung, spinal cord, and brain were collected, immediately frozen in dry ice, and then transfer to -80°C until further processing.

To extract butyrate from plasma or organs, a 1:1 v/v acetonitrile (ACN) to water solution was used. Plasma was mixed 1:1 with the ACN/water solution and centrifuged to remove denatured proteins. Organs were weighed, transferred to Lysing Matrix D tubes, and combined with a 1:1 v/v ACN/water solution. Samples were then lysed using a FastPrep-24 5G homogenizer (MP Biomedicals) and centrifuged. The supernatants were collected for butyrate measurement.

Samples were prepared and derivatized as described in the literature[7,70]. A 3-nitrophenylhydrazine (NPH) stock solution was prepared at 0.02 M in water:ACN 1:1 v/v. A 1-ethyl-3-(3-dimethylaminopropyl)carbodiimide (EDC) stock solution (with 1% pyridine added) was prepared at 0.25 M in water:ACN 1:1 v/v. The internal standard, 4-methylvaleric acid, was added. Samples were mixed with NPH and EDC stocks at a 1:1:1 volume ratio. The mixture was heated in a heating block at 60°C for 30 min. Samples were then filtered through 0.22 μm filters and transferred into HPLC vials, which were stored at 4°C before analysis.

An Agilent 6460 Triple Quad MS-MS was used to detect the derivatized butyrate. Both derivatized butyrate-NPH and 4-methylvaleric-NPH were detected in negative mode. Column: ThermoScientific C18 4.6 × 50 mm, 1.8 μm particle size, at room temperature. Mobile phase A: water with 0.1% v/v formic acid. Mobile phase B: acetonitrile with 0.1% v/v formic acid. Injection volume: 5.0 μL. Flow rate: 0.5 mL/min. Gradient of solvent: 15% mobile phase B at 0.0 min; 100% mobile phase B at 3.5 min; 100% mobile phase B at 6.0 min; 15% mobile phase B at 6.5 min. The MS conditions were optimized using pure butyrate-NPH or 4-methylvaleric-NPH at 1 mM. The fragment voltage was set to 135 V, and the collision energy was 18 V. Multiple reaction monitoring (MRM) of 222 → 137 was assigned to butyrate, and MRM of 250 → 137 was assigned to 4-methylvaleric acid as the internal standard. The ratio between MRM of

butyrate and 4-methylvaleric acid was used to quantify butyrate concentration. The final butyrate content in each organ was normalized by organ weight.

Collagen-antibody inducing arthritis (CAIA) model

BALB/c mice, aged 6 weeks, were purchased from the Jackson Laboratory and housed in the animal facility at the University of Chicago for 2 weeks before immunization.

Mice were orally gavaged with PBS or SerBut (25 mg) once daily starting on day -14 at the age of 8 weeks. CAIA was induced by passive immunization with an anti-collagen antibody cocktail (1 mg per mice, Arthrogen-CIA® 5-Clone Cocktail Kit, Chondrex, Inc.) (on day 0, followed by an intraperitoneal injection of LPS (25 µg) on day 3. Mice were provided with soft (pine) bedding throughout the experiment. Arthritis severity was monitored daily after day 3 using the criteria for clinical scores according to instructions from Chondrex, Inc., as described previously[58].

On day 12, the thickness of mouse fore- and hindpaws was measured to assess the swelling resulting from arthritis. On day 13, mice were sacrificed, and the spleen and hock-draining LNs, including popliteal, axillary, and brachial LNs, were harvested for immunostaining followed by flow cytometry analysis.

The paws were collected for histological analysis, as described previously[58]. In brief, paws were fixed in 2% paraformaldehyde (Thermo Scientific), decalcified in Decalcifer II (Leica), and stored in 70% ethanol until paraffin embedding. Paraffin-embedded paws were sliced into 5 µm-thick sections and stained with hematoxylin and eosin, or Masson's trichrome. The images were scanned with a CRi Panoramic SCAN 40x or MIDI 20x Whole Slide Scanner, or Olympus VS200 Slideview Research Slide Scanner, and analyzed using ImageJ and QuPath software.

Experimental autoimmune encephalomyelitis (EAE) model

C57BL/6 female mice (7-8 weeks old) were purchased from Charles River Laboratories and housed in the animal facility at the University of Chicago for 2 weeks before immunization.

Female C57BL/6 mice, aged 10 weeks, were subcutaneously immunized at the dorsal flanks with an emulsion of MOG_{35-55} in complete Freund's adjuvant (MOG_{35-55}/CFA Emulsion, Hooke Laboratories) on day 0, followed by i.p. administration of pertussis toxin in PBS on both day 0 and day 1. The development of EAE was monitored, and clinical scores were measured daily from day 7 to day 20. The criteria for clinical scores was according to the instructions from Hooke Laboratories and described previously[71].

In the experiment from Fig. 3, Mice were given drinking water containing 100 mM NaBut, L-Serine (L-Ser), or SerBut from day -14 until the end of the study. On day 2 after EAE induction, PBS, NaBut (15 mg, molar equivalent to SerBut), L-Ser (12 mg, molar equivalent to SerBut), or SerBut (24 mg) were administered once daily. In the experiment from Fig. 4, mice were administered of PBS or SerBut (24 mg) twice daily by oral gavage from day 2 after EAE induction.

On day 21 or 22, mice were sacrificed. The spinal cords were collected and separated into three sections for immunofluorescence imaging, cytokine measurement through homogenization, or immunostaining for flow cytometry analysis. Blood was collected through cardiac puncture, and spleen, mesenteric LNs, spinal cord-draining LNs (SC-dLNs, including cervical LNs and iliac LNs), and spleen were harvested. Isolated single-cell suspension were collected for the immunostaining followed by the flow cytometry analysis. Major cytokines from the plasma and spinal cord after homogenization were analyzed by the LEGENDPlex (BioLegend).

Immunofluorescence imaging on spinal cord

Thoracic and lumbar spines of EAE mice were collected. The tissues were fixed in 2% paraformaldehyde (Thermo Scientific) and then stored in 70% ethanol until paraffin embedding.

Paraffin-embedded spinal cords were sliced into 5 μm-thick sections as previously described[71]. The sections were deparaffinized through a series of washes in xylene, ethanol, and double-distilled water, immersing them in each solution for 2 min. Antigen retrieval was performed using 1x pH 6.0 citrate buffer at 50-55°C for 45 min. Sections were blocked for 1 hr at room temperature with PBS containing 0.3% Triton-X and 5% normal goat serum. Primary antibodies against CD45 (clone 30-F11, BioLegend) and MBP (clone ab40390, Abcam) were applied at 1:100 dilution in blocking buffer and incubated for 16 hr at 4°C. Sections were washed and then incubated with donkey anti-rat IgG (H+L) AF647 (A48272, Invitrogen) and donkey anti-rabbit IgG (H+L) AF488 (2340683, Jackson ImmunoResearch) secondary antibodies for 16 hr at 4°C. After further washing, sections were mounted using Fluoromount-G Mounting Medium and imaged with an Olympus IX83 spinning-disc confocal fluorescence microscope. Image processing was performed using ImageJ and QuPath software.

Evaluation of immune responses to vaccination and safety profile of SerBut

Mice were orally gavaged with PBS, SerBut (twice daily, 24 mg/dose), or FTY720 (once daily, 0.02 mg/dose) starting on day -3 until the end of the experiment. On day 0, mice were immunized subcutaneously in the front hocks with 10 μg endotoxin-free ovalbumin (OVA), 50 μg alum, and 5 μg MPLA[58]. Mice were bled on day 9 and day 13, and plasma was analyzed for anti-OVA total IgG antibodies using a mouse anti-OVA IgG antibody assay kit (Chondrex). On day 13, mice were sacrificed, the hock-draining LNs and spleen were harvest and cells were isolated for the immunostaining followed by the flow cytometry analysis. One million cells from each spleen were seeded in a 96-well plate and incubated with OVA at 100 μg/mL for a 3-day restimulation. The supernatant of cell culture was collected, and cytokines were measured using a LEGENDplex™ mouse Th cytokine assay (BioLegend).

In addition, plasma samples collected on day 13 were analyzed using a biochemistry analyzer (Alfa Wassermann Diagnostic Technologies) according to the manufacturer's

instructions. The panel included albumin, alanine amino-transferase, amylase, aspartate amino-transferase, blood urea nitrogen, calcium, creatine kinase, creatine, total bilirubin, and total protein.

Statistical analysis

Statistical analysis and plotting of data were performed using Prism 9.0 (Graphpad), as indicated in the figure legends. One-way ANOVA with Dunnett's or Kruskal-Wallis test (if not normally distributed) for multiple comparisons was used in **Fig. 1C-H, Fig. 3B, D-N,** and **Fig. 5B-G**. Student's t-test was used in **Fig. 2B-D, H-M** and **Fig. 4B, D, F-O**. Two-way ANOVA with Tukey's or Bonferroni's post-test was used in **Fig. 5H-M**. In **Fig. 2B**, **Fig. 3B**, and **Fig. 4B**, the area under curve (AUC) values of clinical scores were compared using one-way ANOVA with Dunnett's post-test, or Student's t test. In **Fig. 3C** and **Fig. 4C**, the probability curve of EAE clinical scores remaining below 1.0 were compared between each two groups using the Log-rank (Mantel-Cox) test. Data represent mean ± s.e.m.; *n* is stated in the figure legend. *$p<0.05$, **$p<0.01$, ***$p<0.001$, ****$p<0.0001$.

Acknowledgements

This work was supported by the Chicago Immunoengineering Innovation Center of the University of Chicago and the Alper Family Fund. We thank Yue Wang from Prof. Melody Swartz's laboratory for providing mouse BMDCs. We thank Dr. Abbey Lauterbach for helping on interpreting histology images. We thank the Cytometry and Antibody Technology Core Facility (Cancer Center Support Grant P30CA014599), the Human Tissue Resource Center, the Integrated Light Microscopy Core, and the Mass Spectrometry Facility (National Science Foundation instrumentation grant CHE-1048528) at the University of Chicago.

Author contributions

J.A.H. oversaw all research. S.C., E.B., and J.A.H. designed most of experiments. S.C., M.M.R., synthesized materials. S.C., E.B., M.M.R., A.S., M.N., K.H., P.A., J.W.R., L.S.S., R.P.W., A.D., and E.A.W. performed experiments. S.C. and E.B. analyzed experiments. S.C., E.B., and J.A.H. wrote the manuscript. All authors contributed to the article and approved the submitted version.

Competing interests

S.C., E.B., M.M.R., E.A.W. and J.A.H. are inventors on a patent filed by the University of Chicago on uses of SerBut.

References

1. Skelly, A.N., Sato, Y., Kearney, S., and Honda, K. (2019). Mining the microbiota for microbial and metabolite-based immunotherapies. Nat. Rev. Immunol. *19*, 305–323. 10.1038/s41577-019-0144-5.

2. Agus, A., Clément, K., and Sokol, H. (2021). Gut microbiota-derived metabolites as central regulators in metabolic disorders. Gut *70*, 1174–1182. 10.1136/gutjnl-2020-323071.

3. Miyauchi, E., Shimokawa, C., Steimle, A., Desai, M.S., and Ohno, H. (2023). The impact of the gut microbiome on extra-intestinal autoimmune diseases. Nat. Rev. Immunol. *23*, 9–23. 10.1038/s41577-022-00727-y.

4. Honda, K., and Littman, D.R. (2016). The microbiota in adaptive immune homeostasis and disease. Nature *535*, 75–84. 10.1038/nature18848.

5. Donohoe, D.R., Garge, N., Zhang, X., Sun, W., O'Connell, T.M., Bunger, M.K., and Bultman, S.J. (2011). The Microbiome and Butyrate Regulate Energy Metabolism and Autophagy in the Mammalian Colon. Cell Metab. *13*, 517–526. 10.1016/j.cmet.2011.02.018.

6. Wells, J.M., Brummer, R.J., Derrien, M., MacDonald, T.T., Troost, F., Cani, P.D., Theodorou, V., Dekker, J., Méheust, A., de Vos, W.M., et al. (2017). Homeostasis of the gut barrier and potential biomarkers. Am. J. Physiol.-Gastrointest. Liver Physiol. *312*, G171–G193. 10.1152/ajpgi.00048.2015.

7. Wang, R., Cao, S., Bashir, M.E.H., Hesser, L.A., Su, Y., Hong, S.M.C., Thompson, A., Culleen, E., Sabados, M., Dylla, N.P., et al. (2022). Treatment of peanut allergy and colitis in mice via the intestinal release of butyrate from polymeric micelles. Nat. Biomed. Eng., 1–18. 10.1038/s41551-022-00972-5.

8. Koh, A., De Vadder, F., Kovatcheva-Datchary, P., and Bäckhed, F. (2016). From Dietary Fiber to Host Physiology: Short-Chain Fatty Acids as Key Bacterial Metabolites. Cell *165*, 1332–1345. 10.1016/j.cell.2016.05.041.

9. Peng, L., Li, Z.-R., Green, R.S., Holzman, I.R., and Lin, J. (2009). Butyrate enhances the intestinal barrier by facilitating tight junction assembly via activation of AMP-activated protein kinase in Caco-2 cell monolayers. J. Nutr. *139*, 1619–1625. 10.3945/jn.109.104638.

10. Peng, L., He, Z., Chen, W., Holzman, I.R., and Lin, J. (2007). Effects of butyrate on intestinal barrier function in a Caco-2 cell monolayer model of intestinal barrier. Pediatr. Res. *61*, 37–41. 10.1203/01.pdr.0000250014.92242.f3.

11. McKay, J.A., and Mathers, J.C. (2011). Diet induced epigenetic changes and their implications for health. Acta Physiol. Oxf. Engl. *202*, 103–118. 10.1111/j.1748-1716.2011.02278.x.

12. Berni Canani, R., Di Costanzo, M., and Leone, L. (2012). The epigenetic effects of butyrate: potential therapeutic implications for clinical practice. Clin. Epigenetics *4*, 4. 10.1186/1868-7083-4-4.

13. Tan, J., McKenzie, C., Potamitis, M., Thorburn, A.N., Mackay, C.R., and Macia, L. (2014). The role of short-chain fatty acids in health and disease. Adv. Immunol. *121*, 91–119. 10.1016/B978-0-12-800100-4.00003-9.

14. Hamer, H.M., Jonkers, D., Venema, K., Vanhoutvin, S., Troost, F.J., and Brummer, R.-J. (2008). Review article: the role of butyrate on colonic function. Aliment. Pharmacol. Ther. *27*, 104–119. 10.1111/j.1365-2036.2007.03562.x.

15. Smith, P.M., Howitt, M.R., Panikov, N., Michaud, M., Gallini, C.A., Bohlooly-Y, M., Glickman, J.N., and Garrett, W.S. (2013). The microbial metabolites, short-chain fatty acids, regulate colonic Treg cell homeostasis. Science *341*, 569–573. 10.1126/science.1241165.

16. Furusawa, Y., Obata, Y., Fukuda, S., Endo, T.A., Nakato, G., Takahashi, D., Nakanishi, Y., Uetake, C., Kato, K., Kato, T., et al. (2013). Commensal microbe-derived butyrate induces the differentiation of colonic regulatory T cells. Nature *504*, 446–450. 10.1038/nature12721.

17. Arpaia, N., Campbell, C., Fan, X., Dikiy, S., van der Veeken, J., deRoos, P., Liu, H., Cross, J.R., Pfeffer, K., Coffer, P.J., et al. (2013). Metabolites produced by commensal bacteria promote peripheral regulatory T-cell generation. Nature *504*, 451–455. 10.1038/nature12726.

18. Meijer, K., de Vos, P., and Priebe, M.G. (2010). Butyrate and other short-chain fatty acids as modulators of immunity: what relevance for health? Curr. Opin. Clin. Nutr. Metab. Care *13*, 715–721. 10.1097/MCO.0b013e32833eebe5.

19. Kaisar, M.M.M., Pelgrom, L.R., van der Ham, A.J., Yazdanbakhsh, M., and Everts, B. (2017). Butyrate Conditions Human Dendritic Cells to Prime Type 1 Regulatory T Cells via both Histone Deacetylase Inhibition and G Protein-Coupled Receptor 109A Signaling. Front. Immunol. *8*, 1429. 10.3389/fimmu.2017.01429.

20. Nastasi, C., Candela, M., Bonefeld, C.M., Geisler, C., Hansen, M., Krejsgaard, T., Biagi, E., Andersen, M.H., Brigidi, P., Ødum, N., et al. (2015). The effect of short-chain fatty acids on human monocyte-derived dendritic cells. Sci. Rep. *5*, 16148. 10.1038/srep16148.

21. Ang, Z., and Ding, J.L. (2016). GPR41 and GPR43 in Obesity and Inflammation – Protective or Causative? Front. Immunol. *7*.

22. Brown, A.J., Goldsworthy, S.M., Barnes, A.A., Eilert, M.M., Tcheang, L., Daniels, D., Muir, A.I., Wigglesworth, M.J., Kinghorn, I., Fraser, N.J., et al. (2003). The Orphan G protein-coupled receptors GPR41 and GPR43 are activated by propionate and other short chain carboxylic acids. J. Biol. Chem. *278*, 11312–11319. 10.1074/jbc.M211609200.

23. Fugger, L., Jensen, L.T., and Rossjohn, J. (2020). Challenges, Progress, and Prospects of Developing Therapies to Treat Autoimmune Diseases. Cell *181*, 63–80. 10.1016/j.cell.2020.03.007.

24. Horta-Baas, G., Romero-Figueroa, M.D.S., Montiel-Jarquín, A.J., Pizano-Zárate, M.L., García-Mena, J., and Ramírez-Durán, N. (2017). Intestinal Dysbiosis and Rheumatoid Arthritis: A Link between Gut Microbiota and the Pathogenesis of Rheumatoid Arthritis. J. Immunol. Res. *2017*, 4835189. 10.1155/2017/4835189.

25. Stoll, M.L., Kumar, R., Morrow, C.D., Lefkowitz, E.J., Cui, X., Genin, A., Cron, R.Q., and Elson, C.O. (2014). Altered microbiota associated with abnormal humoral immune responses to commensal organisms in enthesitis-related arthritis. Arthritis Res. Ther. *16*, 486. 10.1186/s13075-014-0486-0.

26. Jangi, S., Gandhi, R., Cox, L.M., Li, N., von Glehn, F., Yan, R., Patel, B., Mazzola, M.A., Liu, S., Glanz, B.L., et al. (2016). Alterations of the human gut microbiome in multiple sclerosis. Nat. Commun. *7*, 12015. 10.1038/ncomms12015.

27. Cantarel, B.L., Waubant, E., Chehoud, C., Kuczynski, J., DeSantis, T.Z., Warrington, J., Venkatesan, A., Fraser, C.M., and Mowry, E.M. (2015). Gut microbiota in multiple sclerosis: possible influence of immunomodulators. J. Investig. Med. Off. Publ. Am. Fed. Clin. Res. *63*, 729–734. 10.1097/JIM.0000000000000192.

28. Mizuno, M., Noto, D., Kaga, N., Chiba, A., and Miyake, S. (2017). The dual role of short fatty acid chains in the pathogenesis of autoimmune disease models. PloS One *12*, e0173032. 10.1371/journal.pone.0173032.

29. Liu, H., Wang, J., He, T., Becker, S., Zhang, G., Li, D., and Ma, X. (2018). Butyrate: A Double-Edged Sword for Health? Adv. Nutr. Bethesda Md *9*, 21–29. 10.1093/advances/nmx009.

30. Breuer, R.I., Buto, S.K., Christ, M.L., Bean, J., Vernia, P., Paoluzi, P., Di Paolo, M.C., and Caprilli, R. (1991). Rectal irrigation with short-chain fatty acids for distal ulcerative colitis. Preliminary report. Dig. Dis. Sci. *36*, 185–187. 10.1007/BF01300754.

31. Breuer, R.I., Soergel, K.H., Lashner, B.A., Christ, M.L., Hanauer, S.B., Vanagunas, A., Harig, J.M., Keshavarzian, A., Robinson, M., Sellin, J.H., et al. (1997). Short chain fatty acid rectal irrigation for left-sided ulcerative colitis: a randomised, placebo controlled trial. Gut *40*, 485–491. 10.1136/gut.40.4.485.

32. Sher, G.D., Ginder, G.D., Little, J., Yang, S., Dover, G.J., and Olivieri, N.F. (1995). Extended therapy with intravenous arginine butyrate in patients with beta-hemoglobinopathies. N. Engl. J. Med. *332*, 1606–1610. 10.1056/NEJM199506153322404.

33. Vernia, P., Cittadini, M., Caprilli, R., and Torsoli, A. (1995). Topical treatment of refractory distal ulcerative colitis with 5-ASA and sodium butyrate. Dig. Dis. Sci. *40*, 305–307. 10.1007/BF02065414.

34. MILLARD, A.L., MERTES, P.M., ITTELET, D., VILLARD, F., JEANNESSON, P., and BERNARD, J. (2002). Butyrate affects differentiation, maturation and function of human monocyte-derived dendritic cells and macrophages. Clin. Exp. Immunol. *130*, 245–255. 10.1046/j.0009-9104.2002.01977.x.

35. Bröer, S. (2008). Amino acid transport across mammalian intestinal and renal epithelia. Physiol. Rev. *88*, 249–286. 10.1152/physrev.00018.2006.

36. Tayarani, I., Lefauconnier, J.M., Roux, F., and Bourre, J.M. (1987). Evidence for an alanine, serine, and cysteine system of transport in isolated brain capillaries. J. Cereb. Blood Flow Metab. Off. J. Int. Soc. Cereb. Blood Flow Metab. *7*, 585–591. 10.1038/jcbfm.1987.109.

37. Hawkins, R.A., O'Kane, R.L., Simpson, I.A., and Viña, J.R. (2006). Structure of the blood-brain barrier and its role in the transport of amino acids. J. Nutr. *136*, 218S-26S. 10.1093/jn/136.1.218S.

38. Montaser, A.B., Järvinen, J., Löffler, S., Huttunen, J., Auriola, S., Lehtonen, M., Jalkanen, A., and Huttunen, K.M. (2020). L-Type Amino Acid Transporter 1 Enables the Efficient Brain Delivery of Small-Sized Prodrug across the Blood-Brain Barrier and into Human and Mouse Brain Parenchymal Cells. ACS Chem. Neurosci. *11*, 4301–4315. 10.1021/acschemneuro.0c00564.

39. Maeda, Y., and Takeda, K. (2017). Role of Gut Microbiota in Rheumatoid Arthritis. J. Clin. Med. *6*, 60. 10.3390/jcm6060060.

40. Kim, D.S., Kwon, J.-E., Lee, S.H., Kim, E.K., Ryu, J.-G., Jung, K.-A., Choi, J.-W., Park, M.-J., Moon, Y.-M., Park, S.-H., et al. (2018). Attenuation of Rheumatoid Inflammation by Sodium Butyrate Through Reciprocal Targeting of HDAC2 in Osteoclasts and HDAC8 in T Cells. Front. Immunol. *9*, 1525. 10.3389/fimmu.2018.01525.

41. Rosser, E.C., Piper, C.J.M., Matei, D.E., Blair, P.A., Rendeiro, A.F., Orford, M., Alber, D.G., Krausgruber, T., Catalan, D., Klein, N., et al. (2020). Microbiota-Derived Metabolites Suppress Arthritis by Amplifying Aryl-Hydrocarbon Receptor Activation in Regulatory B Cells. Cell Metab. *31*, 837-851.e10. 10.1016/j.cmet.2020.03.003.

42. Terato, K., Hasty, K.A., Reife, R.A., Cremer, M.A., Kang, A.H., and Stuart, J.M. (1992). Induction of arthritis with monoclonal antibodies to collagen. J. Immunol. Baltim. Md 1950 *148*, 2103–2108.

43. Hutamekalin, P., Saito, T., Yamaki, K., Mizutani, N., Brand, D.D., Waritani, T., Terato, K., and Yoshino, S. (2009). Collagen antibody-induced arthritis in mice: Development of a new arthritogenic 5-clone cocktail of monoclonal anti-type II collagen antibodies. J. Immunol. Methods *343*, 49–55. 10.1016/j.jim.2009.01.009.

44. Rowley, M.J., Nandakumar, K.S., and Holmdahl, R. (2008). The role of collagen antibodies in mediating arthritis. Mod. Rheumatol. *18*, 429–441. 10.1007/s10165-008-0080-x.

45. Kalampokis, I., Yoshizaki, A., and Tedder, T.F. (2013). IL-10-producing regulatory B cells (B10 cells) in autoimmune disease. Arthritis Res. Ther. *15*, S1. 10.1186/ar3907.

46. Cosorich, I., Dalla-Costa, G., Sorini, C., Ferrarese, R., Messina, M.J., Dolpady, J., Radice, E., Mariani, A., Testoni, P.A., Canducci, F., et al. (2017). High frequency of intestinal TH17 cells correlates with microbiota alterations and disease activity in multiple sclerosis. Sci. Adv. *3*, e1700492. 10.1126/sciadv.1700492.

47. Swidsinski, A., Dörffel, Y., Loening-Baucke, V., Gille, C., Göktas, Ö., Reißhauer, A., Neuhaus, J., Weylandt, K.-H., Guschin, A., and Bock, M. (2017). Reduced Mass and Diversity of the Colonic Microbiome in Patients with Multiple Sclerosis and Their Improvement with Ketogenic Diet. Front. Microbiol. *8*, 1141. 10.3389/fmicb.2017.01141.

48. Cekanaviciute, E., Yoo, B.B., Runia, T.F., Debelius, J.W., Singh, S., Nelson, C.A., Kanner, R., Bencosme, Y., Lee, Y.K., Hauser, S.L., et al. (2017). Gut bacteria from multiple sclerosis patients modulate human T cells and exacerbate symptoms in mouse models. Proc. Natl. Acad. Sci. *114*, 10713–10718. 10.1073/pnas.1711235114.

49. Berer, K., Gerdes, L.A., Cekanaviciute, E., Jia, X., Xiao, L., Xia, Z., Liu, C., Klotz, L., Stauffer, U., Baranzini, S.E., et al. (2017). Gut microbiota from multiple sclerosis patients enables spontaneous autoimmune encephalomyelitis in mice. Proc. Natl. Acad. Sci. *114*, 10719–10724. 10.1073/pnas.1711233114.

50. Stanisavljević, S., Dinić, M., Jevtić, B., Đedović, N., Momčilović, M., Đokić, J., Golić, N., Mostarica Stojković, M., and Miljković, Đ. (2018). Gut Microbiota Confers Resistance of Albino Oxford Rats to the Induction of Experimental Autoimmune Encephalomyelitis. Front. Immunol. *9*, 942. 10.3389/fimmu.2018.00942.

51. Miyake, S., Kim, S., Suda, W., Oshima, K., Nakamura, M., Matsuoka, T., Chihara, N., Tomita, A., Sato, W., Kim, S.-W., et al. (2015). Dysbiosis in the Gut Microbiota of Patients with Multiple Sclerosis, with a Striking Depletion of Species Belonging to Clostridia XIVa and IV Clusters. PLOS ONE *10*, e0137429. 10.1371/journal.pone.0137429.

52. Haghikia, A., Jörg, S., Duscha, A., Berg, J., Manzel, A., Waschbisch, A., Hammer, A., Lee, D.-H., May, C., Wilck, N., et al. (2015). Dietary Fatty Acids Directly Impact Central Nervous System Autoimmunity via the Small Intestine. Immunity *43*, 817–829. 10.1016/j.immuni.2015.09.007.

53. Chen, T., Noto, D., Hoshino, Y., Mizuno, M., and Miyake, S. (2019). Butyrate suppresses demyelination and enhances remyelination. J. Neuroinflammation *16*, 165. 10.1186/s12974-019-1552-y.

54. Zhu, B., Bando, Y., Xiao, S., Yang, K., Anderson, A.C., Kuchroo, V.K., and Khoury, S.J. (2007). CD11b+Ly-6C(hi) suppressive monocytes in experimental autoimmune encephalomyelitis. J. Immunol. Baltim. Md 1950 *179*, 5228–5237. 10.4049/jimmunol.179.8.5228.

55. Schulze-Topphoff, U., Varrin-Doyer, M., Pekarek, K., Spencer, C.M., Shetty, A., Sagan, S.A., Cree, B.A.C., Sobel, R.A., Wipke, B.T., Steinman, L., et al. (2016). Dimethyl fumarate treatment induces adaptive and innate immune modulation independent of Nrf2. Proc. Natl. Acad. Sci. U. S. A. *113*, 4777–4782. 10.1073/pnas.1603907113.

56. Ayzenberg, I., Hoepner, R., and Kleiter, I. (2016). Fingolimod for multiple sclerosis and emerging indications: appropriate patient selection, safety precautions, and special considerations. Ther. Clin. Risk Manag. *12*, 261–272. 10.2147/TCRM.S65558.

57. Chun, J., and Hartung, H.-P. (2010). Mechanism of Action of Oral Fingolimod (FTY720) in Multiple Sclerosis. Clin. Neuropharmacol. *33*, 91–101. 10.1097/WNF.0b013e3181cbf825.

58. Yuba, E., Budina, E., Katsumata, K., Ishihara, A., Mansurov, A., Alpar, A.T., Watkins, E.A., Hosseinchi, P., Reda, J.W., Lauterbach, A.L., et al. (2021). Suppression of Rheumatoid Arthritis by Enhanced Lymph Node Trafficking of Engineered Interleukin-10 in Murine Models. Arthritis Rheumatol. *73*, 769–778. 10.1002/art.41585.

59. Zhang, L., Liu, C., Jiang, Q., and Yin, Y. (2021). Butyrate in Energy Metabolism: There Is Still More to Learn. Trends Endocrinol. Metab. *32*, 159–169. 10.1016/j.tem.2020.12.003.

60. Singh, N., Gurav, A., Sivaprakasam, S., Brady, E., Padia, R., Shi, H., Thangaraju, M., Prasad, P.D., Manicassamy, S., Munn, D.H., et al. (2014). Activation of the receptor (Gpr109a) for niacin and the commensal metabolite butyrate suppresses colonic inflammation and carcinogenesis. Immunity *40*, 128–139. 10.1016/j.immuni.2013.12.007.

61. Newmark, H.L., Lupton, J.R., and Young, C.W. (1994). Butyrate as a differentiating agent: pharmacokinetics, analogues and current status. Cancer Lett. *78*, 1–5. 10.1016/0304-3835(94)90023-X.

62. Cummings, J.H., Pomare, E.W., Branch, W.J., Naylor, C.P., and Macfarlane, G.T. (1987). Short chain fatty acids in human large intestine, portal, hepatic and venous blood. Gut *28*, 1221–1227. 10.1136/gut.28.10.1221.

63. Chang, P.V., Hao, L., Offermanns, S., and Medzhitov, R. (2014). The microbial metabolite butyrate regulates intestinal macrophage function via histone deacetylase inhibition. Proc. Natl. Acad. Sci. *111*, 2247–2252. 10.1073/pnas.1322269111.

64. Scott, N.A., Andrusaite, A., Andersen, P., Lawson, M., Alcon-Giner, C., Leclaire, C., Caim, S., Le Gall, G., Shaw, T., Connolly, J.P.R., et al. (2018). Antibiotics induce sustained dysregulation of intestinal T cell immunity by perturbing macrophage homeostasis. Sci. Transl. Med. *10*, eaao4755. 10.1126/scitranslmed.aao4755.

65. Sansom, D.M. (2000). CD28, CTLA-4 and their ligands: who does what and to whom? Immunology *101*, 169–177. 10.1046/j.1365-2567.2000.00121.x.

66. Linsley, P.S., and Ledbetter, J.A. (1993). The role of the CD28 receptor during T cell responses to antigen. Annu. Rev. Immunol. *11*, 191–212. 10.1146/annurev.iy.11.040193.001203.

67. Walker, L.S.K., and Sansom, D.M. (2011). The emerging role of CTLA4 as a cell-extrinsic regulator of T cell responses. Nat. Rev. Immunol. *11*, 852–863. 10.1038/nri3108.

68. Didierlaurent, A.M., Morel, S., Lockman, L., Giannini, S.L., Bisteau, M., Carlsen, H., Kielland, A., Vosters, O., Vanderheyde, N., Schiavetti, F., et al. (2009). AS04, an Aluminum Salt- and TLR4 Agonist-Based Adjuvant System, Induces a Transient Localized Innate Immune Response Leading to Enhanced Adaptive Immunity1. J. Immunol. *183*, 6186–6197. 10.4049/jimmunol.0901474.

69. Lutz, M.B., Kukutsch, N., Ogilvie, A.L.J., Rößner, S., Koch, F., Romani, N., and Schuler, G. (1999). An advanced culture method for generating large quantities of highly pure dendritic cells from mouse bone marrow. J. Immunol. Methods *223*, 77–92. 10.1016/S0022-1759(98)00204-X.

70. Torii, T., Kanemitsu, K., Wada, T., Itoh, S., Kinugawa, K., and Hagiwara, A. (2010). Measurement of short-chain fatty acids in human faeces using high-performance liquid chromatography: specimen stability. Ann. Clin. Biochem. *47*, 447–452. 10.1258/acb.2010.010047.

71. Ishihara, A., Ishihara, J., Watkins, E.A., Tremain, A.C., Nguyen, M., Solanki, A., Katsumata, K., Mansurov, A., Budina, E., Alpar, A.T., et al. (2021). Prolonged residence of an albumin–IL-4 fusion protein in secondary lymphoid organs ameliorates experimental autoimmune encephalomyelitis. Nat. Biomed. Eng. *5*, 387–398. 10.1038/s41551-020-00627-3.

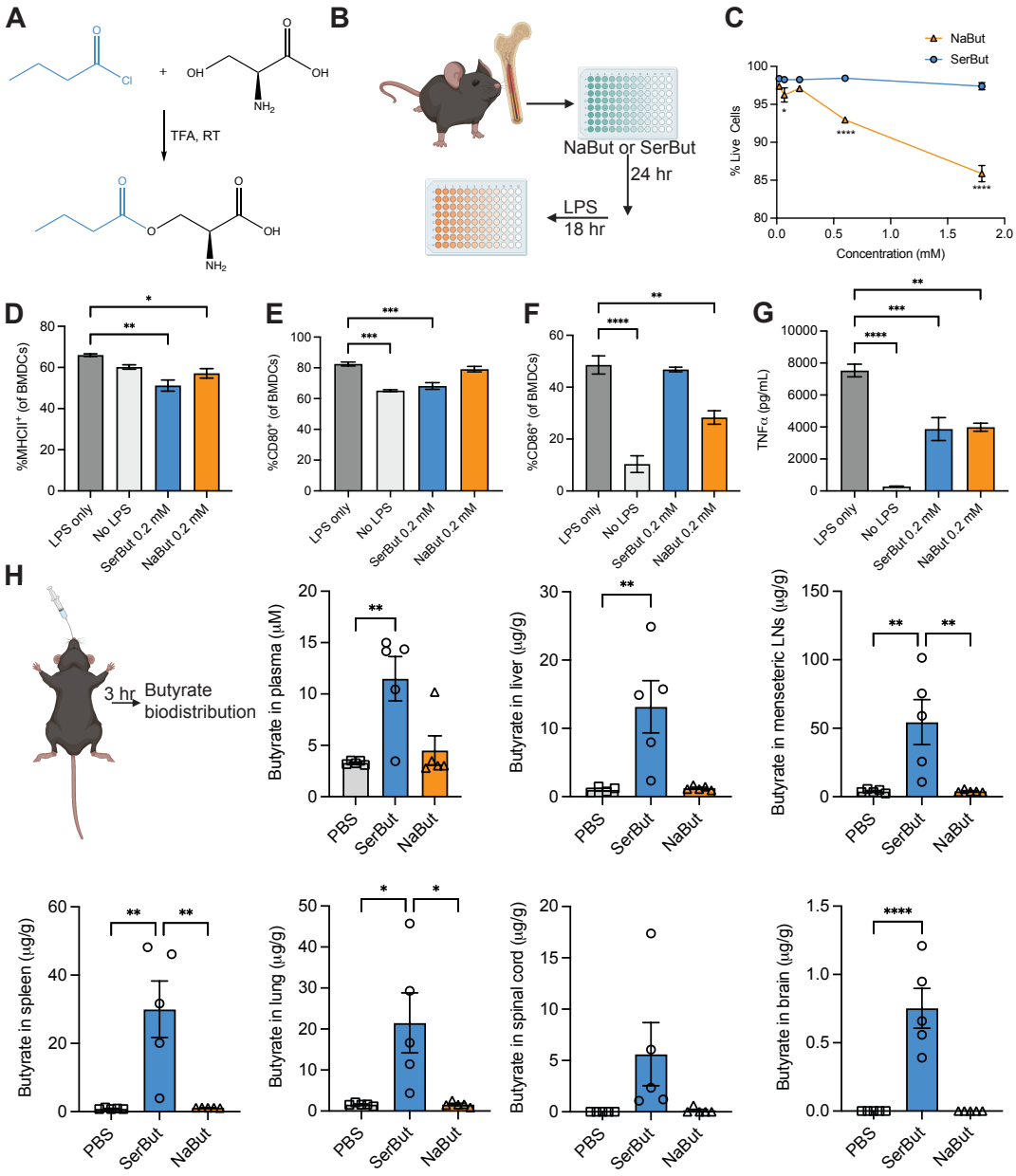

Figure 1 | A. Chemical synthesis of serine conjugate with butyrate (SerBut). **B.** Experimental schema on bone marrow-derived dendritic cells (BMDCs) incubated with sodium butyrate (NaBut) or SerBut at a series of concentrations for 24 hr, followed by LPS stimulation for 18 hr. **C.** Percentage of live BMDCs after treatment. **D-F,** Percentage of CD80$^+$, CD86$^+$, or MHCII$^+$ cells of BMDCs analyzed by flow cytometry. **G.** TNFα concentration in the cell culture supernatant of BMDCs. *n* = 3 and the experiments were repeated twice. **H.** Butyrate biodistribution after SerBut or NaBut oral administration to C57BL/6 mice. The amount of butyrate was detected and quantified in the plasma, liver, mesenteric lymph nodes (mLNs), spleen, lung, spinal cord, and brain. Blood was collected by cheek bleeding at 3 hr post oral gavage. Mice were sacrificed and perfused at 3 hr post oral gavage, and organs were collected for butyrate quantification. Butyrate was derivatized with 3-nitrophenylhydrazine and quantified by LC-MS/MS. *n* = 5 mice per group. Data represent mean ± s.e.m. Statistical analyses were performed using a one-way ANOVA with Dunnett's test. *p<0.05, **p<0.01, ***p<0.001, ****p<0.0001. Figure 1B, H were created with BioRender.com.

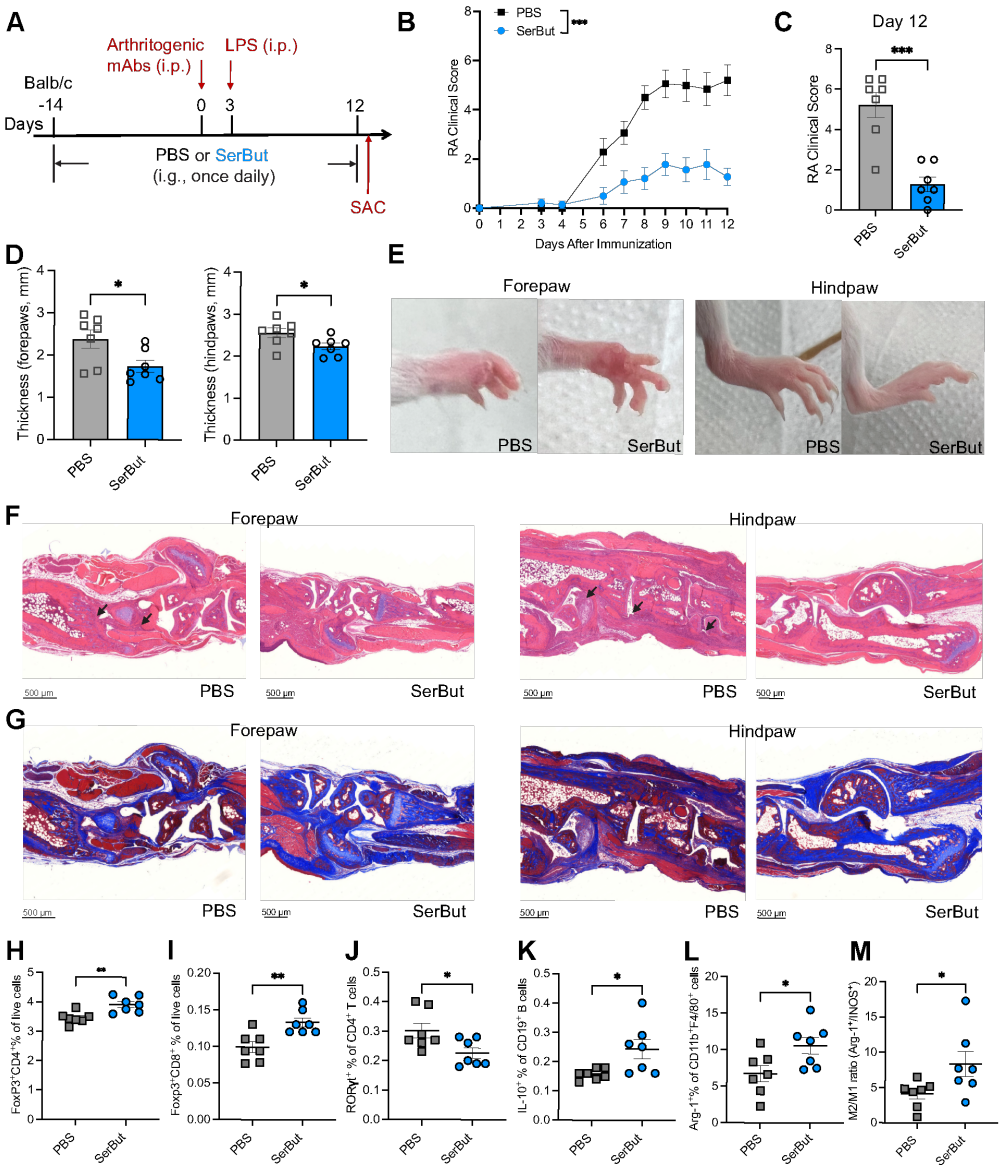

Figure 2 | SerBut suppresses arthritis development. A. Experimental schema of the collagen antibody-induced arthritis (CAIA) model. Mice were orally gavaged with PBS or SerBut (25 mg) once daily starting on day -14. CAIA was induced by passive immunization with anti-collagen antibody cocktails on day 0, followed by intraperitoneal injection of lipopolysaccharide (LPS). **B.** Arthritis scores in mice measured daily after the immunization. **C.** Arthritis scores from PBS or SerBut treated mice on day 12. **D.** The thickness of forepaws or hindpaws measured on day 12 from mice treated with PBS or SerBut. **E.** Representative photos of paws after treatment. **F.** Representative images of mouse joints from paws stained with hematoxylin and eosin on day 12 in each treatment group. Bar = 500 μm. Arrows indicate immune cell infiltration. **G**. Representative images of mouse joints from paws stained with Masson's trichrome on day 12. Bar = 500 μm. Blue represents collagen staining. **H-I.** Percentage of Foxp3$^+$ regulatory CD4$^+$ T cells (H) or Foxp3$^+$ regulatory CD8$^+$ T cells (I) of live cells in the spleen measured by flow cytometry. **J-M.** Percentage of RORγt$^+$ of CD4$^+$ T cells (J) and IL-10$^+$ of CD19$^+$ B cells (K), as well as Arg-1$^+$ of CD11b$^+$F4/80$^+$ macrophages (L), and M2/M1 macrophage ratio (M) in the hock draining LNs. *n* = 7 mice per group. Data represent mean ± s.e.m. Statistical analyses were performed using Student's t-test. *p<0.05, **p<0.01, ***p<0.001.

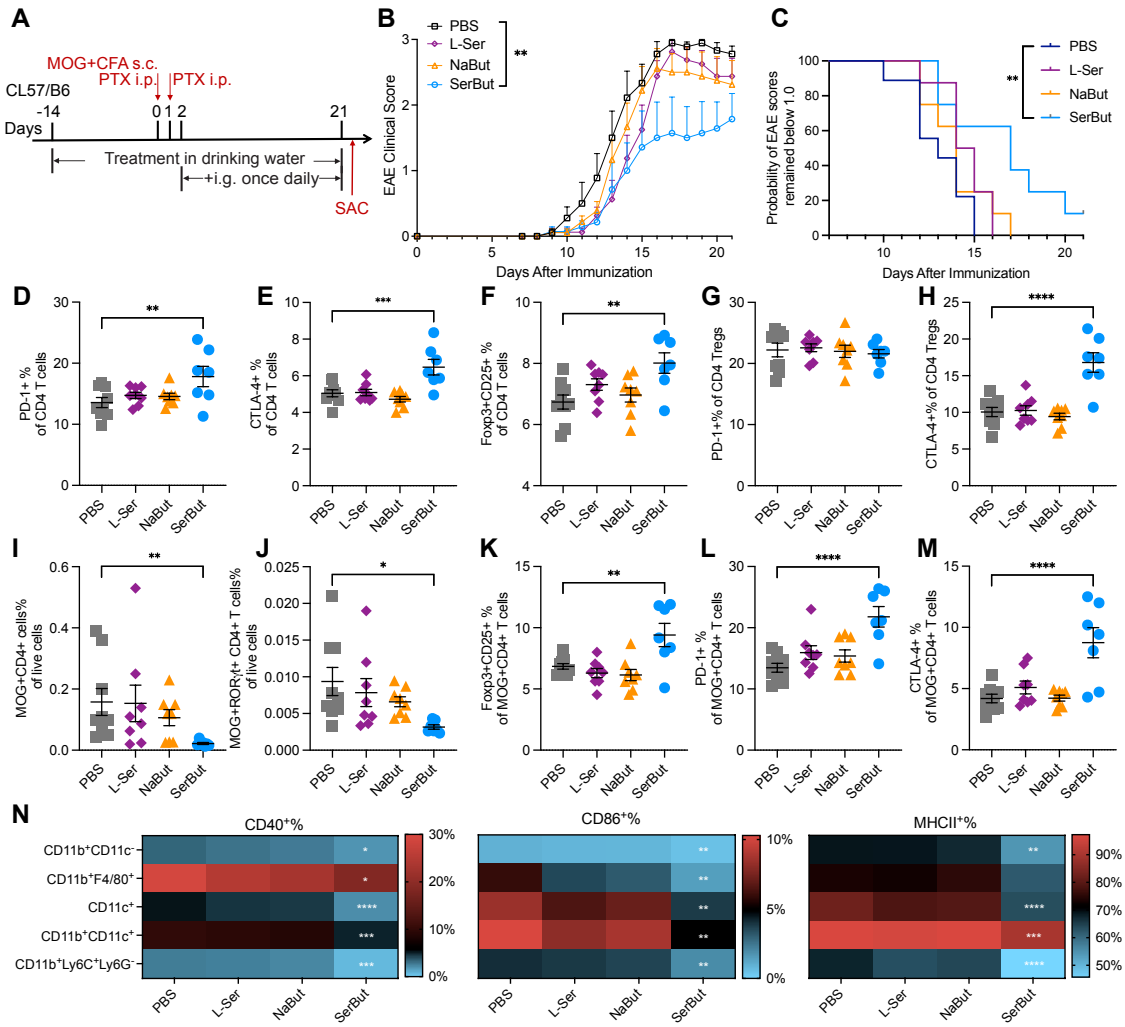

Figure 3 | SerBut ameliorates EAE development more effectively than free butyrate or serine. A. Experimental schema. EAE was induced in C57BL/6 mice using MOG_{35-55}/CFA with pertussis toxin. Mice were given drinking water containing 100 mM NaBut, L-Serine (L-Ser), or SerBut from day -14 until the end of the study. On day 2 after EAE induction, PBS, NaBut (15 mg, molar equivalent to SerBut), L-Ser (12 mg, molar equivalent to SerBut), or SerBut (24 mg) were administered once daily. **B.** Disease progression as indicated by the clinical score. The areas under the curve were compared, and statistical analyses were performed using a one-way ANOVA with Dunnett's test. **C.** The probability of EAE clinical scores remaining below 1.0 for the three groups. Statistical analysis was performed using the Log-rank (Mantel-Cox) test comparing every two groups. **D-M.** Phenotypes of $CD4^+$ T cells from the spinal cord-draining lymph nodes (SC-dLNs, i.e. the iliac and cervical LNs), including the percentage of PD-1^+ (D), CTLA-4^+ (E), or $Foxp3^+CD25^+$ (F) of total $CD4^+$ T cells; PD-1^+ (G) or CTLA-4^+ (H) of $Foxp3^+CD25^+CD4^+$ Tregs; the percentage of MOG tetramer-positive $CD4^+$ (I) or $CD4^+ROR\gamma t^+$ (J) T cells of total live cells; and $Foxp3^+CD25^+$ (K), PD-1^+ (L), CTLA-4^+ (M) of MOG tetramer-positive $CD4^+$ T cells. **N.** Heatmap of the percentage of co-stimulatory molecule ($CD40^+$ or $CD86^+$) or $MHCII^+$ cells of myeloid cells in the SC-dLNs, indicated by the color as shown in the corresponding scale bar. Data represent mean ± s.e.m. Statistical analyses were compared between PBS and each treatment group using one-way ANOVA with Dunnett's test or Kruskal-Wallis test (if not normally distributed). n = 8 mice per group. *p<0.05, **p<0.01, ***p<0.001, ****p<0.0001.

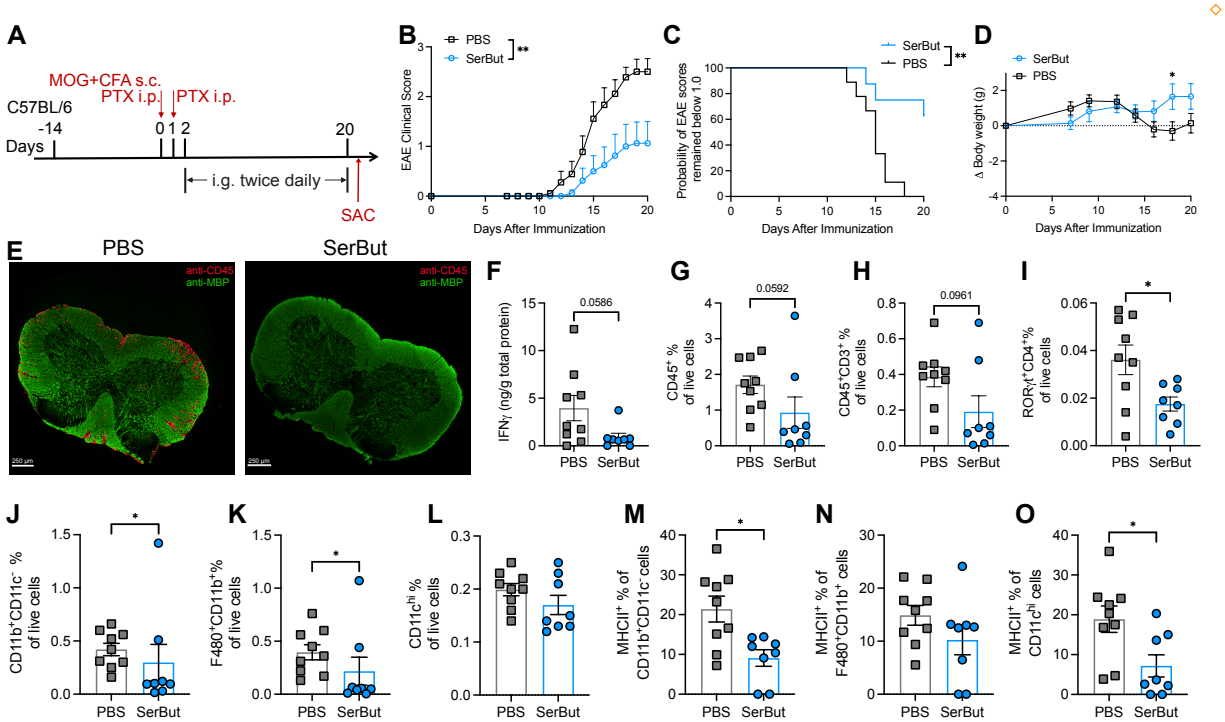

Figure 4 | Twice daily gavage of SerBut post EAE induction suppressed disease. progression. A. Experimental schema. EAE was induced in C57BL/6 mice using MOG_{35-55}/CFA with pertussis toxin. On day 2 after EAE induction, PBS (n=9) or SerBut (n=8) at 24 mg/dose were administered twice daily by gavage. **B.** Disease progression as indicated by the clinical score. The areas under the curve were compared, and statistical analyses were performed using Student's t-test. **C.** The probability of EAE clinical scores remaining below 1.0 in the three groups. Statistical analysis was performed using the Log-rank (Mantel-Cox) test. **D.** Body weight changes. **E.** Representative immunofluorescence images of spinal cord sections from mice treated with PBS or SerBut. Red: anti-CD45 staining; green: anti-myelin basic protein (MBP) staining. Bar = 250 μm. **F.** The concentration of IFN**γ** normalized by the total protein in the spinal cord homogenized supernatant. **G-L.** The percentage of $CD45^+$ (G), $CD45^+CD3^+$(H), $ROR\gamma t^+CD4^+$(I), $CD11b^+CD11c^-$(J), $F4/80^+CD11b^+$ (K), and $CD11c^{hi}$(L) of live cells in the spinal cord. **M-O.** The percentage of $MHCII^+$ of $CD11b^+CD11c^-$(M), $F4/80^+CD11b^+$ (N), or $CD11c^{hi}$(O) cells in the spinal cord. Data represent mean ± s.e.m. Statistical analyses were performed using Student's t-test. *p<0.05, **p<0.01, ***p<0.001, ****p<0.0001.

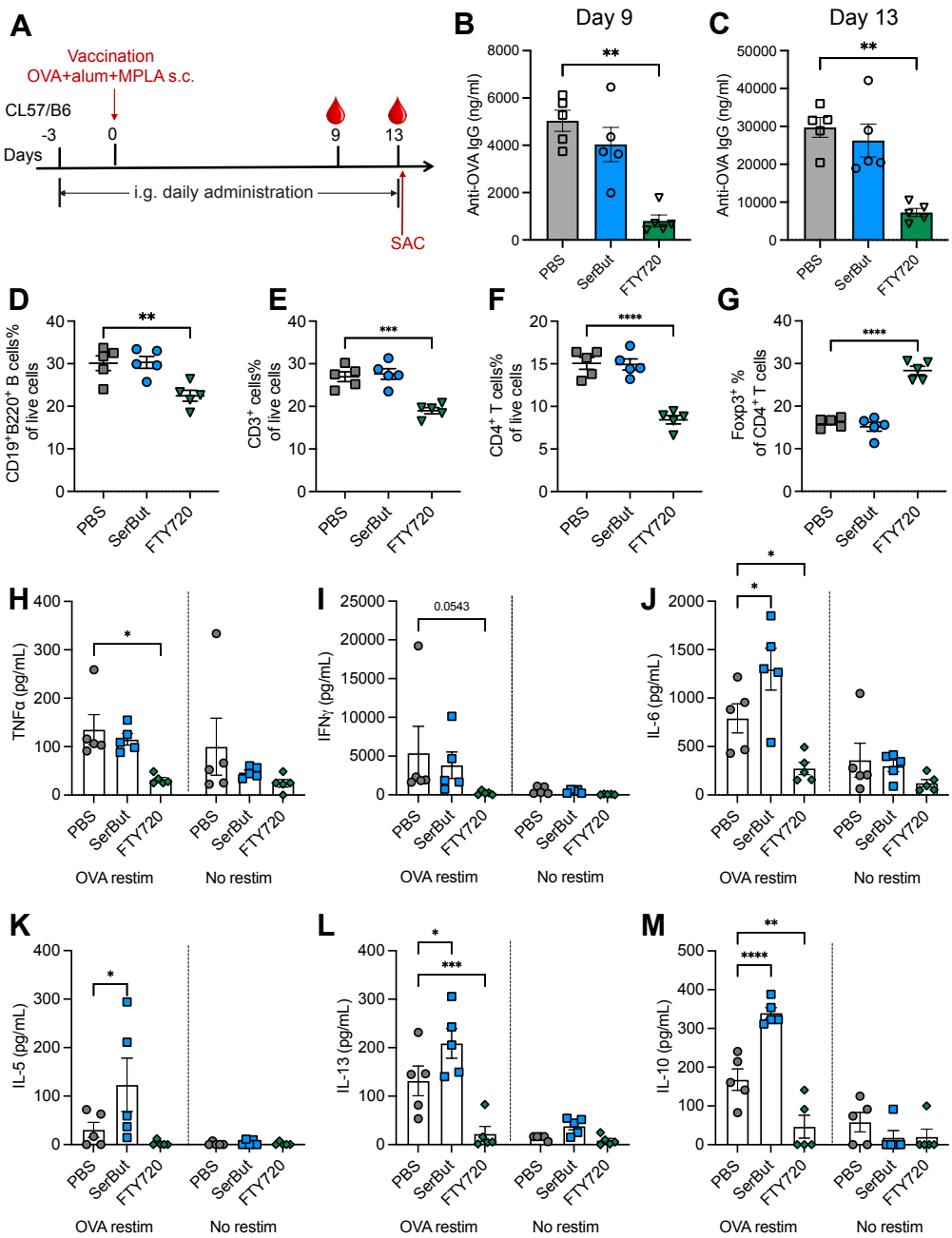

Figure 5 | SerBut does not impact immune responses to vaccination compared to FTY720. A. Experimental schema. Mice were orally gavaged with PBS, SerBut (twice daily, 25 mg/dose), or FTY720 (once daily, 0.02 mg/dose) starting on day -3 until the end of the experiment. On day 0, mice were immunized subcutaneously in the front hocks with 10 µg endotoxin-free ovalbumin (OVA), 50 µg ALUM, and 5 µg MPLA. **B, C.** Mice were bled on day 9 (B) and day 13 (C), and plasma was analyzed for anti-OVA IgG antibodies. **D-G.** The percentages of $CD19^+B220^+$ (D), $CD3^+$ (E), $CD4^+$ (F) of total live cells and $Foxp3^+$ of $CD4^+$ T cells (G) in the spleen. **H-M.** Production of cytokines TNFα (H), IFNγ (I), IL-6 (J), IL-5 (K), IL-13 (L), and IL-10 (M), measured in the supernatant of isolated splenocytes upon restimulation with OVA protein for 3 days. Data represent mean ± s.e.m. Statistical analyses were performed using one-way ANOVA (B-G) or two-way ANOVA (H-M) with Dunnett's post hoc test. *p<0.05, **p<0.01, ***p<0.001, ****p<0.0001.